

Flexible Beam-Like Structures - Experimental Investigation and Modeling of Cables

Vanessa Dörlich, Joachim Linn and Stefan Diebels

1 Introduction

Flexible beam-like structures such as cables or hoses have various applications ranging from everyday to industrial use. Their main function is of course the conduction of electric current, gas, oil or other liquids. But the number of applications where cables and hoses move or have structural functions, e.g. in assembly robots or submarine cables, rises constantly [24, 25]. Therefore, their mechanical properties gain importance [4, 5, 13]. More precisely, the mechanical behavior determines the handling, operational lifetime and failure of cables and hoses [12, 19]. This contribution deals with the experimental investigation and modeling of slender, flexible structures using the example of cables.

We are looking for a model which is complex enough to cover the various effects that occur when cables are loaded mechanically. However, the model parameters have to be accessible in suitable experiments. The optimum in our case is the description of the mechanical behavior on the macroscopic scale, i.e. based on the sectional quantities of the beam. The effects are modeled by formulating the corresponding constitutive laws in the sectional quantities as well. The model parameters are then effective stiffness parameters, which can be obtained from well-known experiments for beam-like specimens. This procedure makes use of the classical framework of continuum mechanics [11] and the possibility to reduce slender objects such as cables to one-dimensional continua.

Section 2 deals with the experimental investigation and phenomena of cables under mechanical load. Three types of load cases are relevant in this context: uniaxial

V. Dörlich (✉) · J. Linn
Fraunhofer ITWM, Fraunhofer-Platz 1, 67663 Kaiserslautern, Germany
e-mail: vanessa.doerlich@itwm.fraunhofer.de

J. Linn
e-mail: joachim.linn@itwm.fraunhofer.de

S. Diebels
Universität des Saarlandes, Campus A4.2, 66123 Saarbrücken, Germany
e-mail: s.diebels@mx.uni-saarland.de

tension, torsion and bending. Classical experiments representing these load cases are used to characterize the mechanical behavior of cables in a first step. Material effects resulting from the structure of cables will be observed.

In this work, we assume the cables' cross sections to be circular and isotropic. Furthermore, we model their mechanical behavior based on the sectional quantities with the Cosserat rod theory [1, 18, 20]. Its essential parts are geometrically exact kinematics, balance equations that govern the equilibrium of sectional forces and moments and constitutive laws that give the relations between objective deformation measures and sectional quantities. Section 3 will describe these more thoroughly.

2 Experiments for Flexible Beam-Like Structures

Executing suitable experiments is an important part of modeling the behavior of structural elements under mechanical load. Sections 2.1, 2.2 and 2.3 show characteristic results and phenomena of cables undergoing the three basic deformation modes uniaxial tension, torsion and bending [22]. The described experiments allow access to the elastic model parameters, i.e. the tensile, torsional and bending stiffnesses [7]. Furthermore, they already illustrate inelastic behavior when the experiments are executed cyclically.

2.1 Uniaxial Tensile Tests

The uniaxial tensile test is the most common experiment for beam-like specimens as well as the characterization of bulk materials. Its boundary conditions are shown in Fig. 1. It is widely used for determining elastic parameters like the Young's modulus E or plastic characteristics such as the yield strength or strain hardening. Usually, these characteristics are taken as material parameters from stress-strain curves, where normalization on the geometrical properties, i.e. the specimen's cross section area and length, is applied. This is reasonable for homogeneous, isotropic materials. In the case of cables and hoses, however, where properties strongly depend on the direction of load, we use force-displacement curves to calculate the tensile stiffness $(EA)_T$, where the cross section area A is still included. As the following results will show, it makes sense to characterize the cable's behavior with this parameter combining material and geometrical properties.

Despite its simplicity, the uniaxial tensile test yields a lot of information about the cable's deformation behavior, especially when executed cyclically. Figure 1 (right) shows the result of a cyclic uniaxial tensile test of a cable with a diameter of 2.8 mm and initial free length of 32 mm, where the uniaxial tensile force F_T is plotted over the measured machine displacement Δl . In order to illustrate the difference between

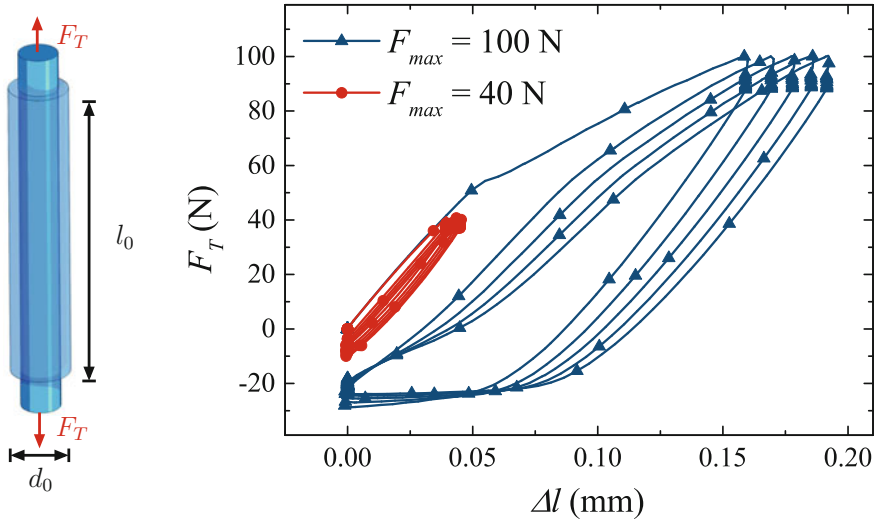


Fig. 1 Uniaxial tensile test: schematic drawing of the boundary conditions (**left**) and exemplary results of a cyclic experiment on a cable showing elastic behavior for $F_{max} = 40$ N and plastic behavior for $F_{max} = 100$ N (**right**)

elastic and inelastic behavior, two curves are shown. One results from a procedure with a maximum load of 40 N and the other one from loading up to 100 N. If the larger maximum force is applied, a bend in the first loading path, denoting the yield point at approximately 54 N and plastic hysteresis loops occur. For cyclic loading below the yield point, loading and unloading paths coincide and no bend occurs in the load-displacement diagram, i.e. the behavior is elastic in this range. The uniaxial tensile stiffness is calculated by applying a linear fit in the elastic range according to

$$F_T = (EA)_T \frac{\Delta l}{l_0}, \quad (1)$$

using the original length l_0 of the specimen.

2.2 Torsion Experiments

Similar to the uniaxial tensile test, the torsion test enables access to the torsional stiffness of a beam-like structure in the elastic range and information about plasticity effects from cyclic loading. The boundary conditions are shown in Fig. 2 (left) and the resulting diagram of torsional moment over torsional angle is shown in Fig. 2 (right) for a cable of 2.8 mm diameter and an initial free length of 33 mm. The result is strongly nonlinear and inelastic with a first load curve that differs from the following

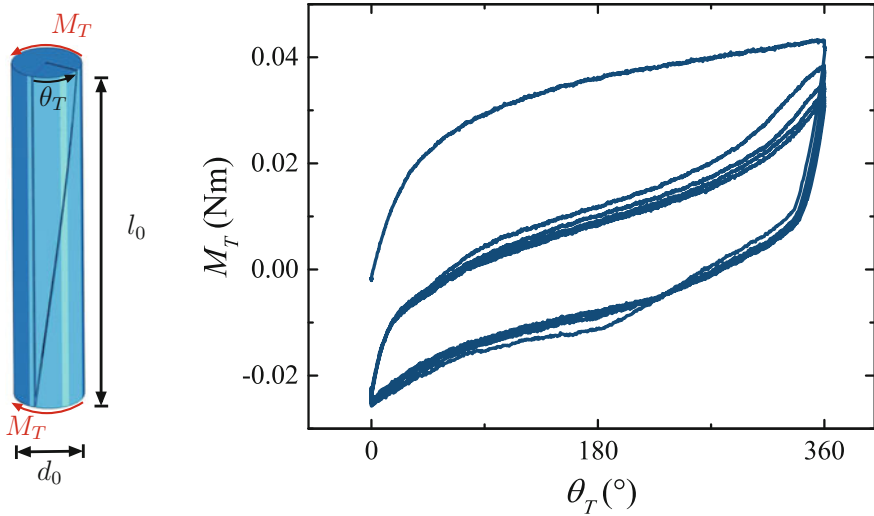


Fig. 2 Torsion test: schematic drawing of the boundary conditions (**left**) and exemplary results of a cyclic experiment on a cable showing plastic behavior for $\theta_{T,max} = 360^\circ$ (**right**)

load paths. The first loading shows again a bend that can be interpreted as the yield point of the specimen. During unloading, a torsional moment in the opposite direction is necessary to reach the original position of 0° torsional angle. The torsional stiffness $(GJ)_T$ is estimated with the help of a linear fit in the elastic range according to

$$M_T = (GJ)_T \frac{\theta_T}{l_0}, \quad (2)$$

where G denotes the shear modulus and J the polar moment of inertia.

2.3 Bending Experiments

Three Point Bending Experiments

It is state of the art to use three point bending experiments [22] to investigate the behavior of cables undergoing bending deformation [7]. The theoretical boundary conditions are shown in Fig. 3 (left). In this experiment, the force F_B on the specimen, which is necessary to reach a certain deflection $w(z = l_0/2)$, is measured in the middle of the specimen. The evaluation of the bending stiffness $(EI)_B$ in this experiment is based on the Euler–Bernoulli assumptions stating that the beam’s cross sections remain planar and normal to the beam’s centerline after deformation. Furthermore, it is only valid for small deflections of sufficiently slender beams. Then, the bending stiffness can be evaluated from a linear fit according to

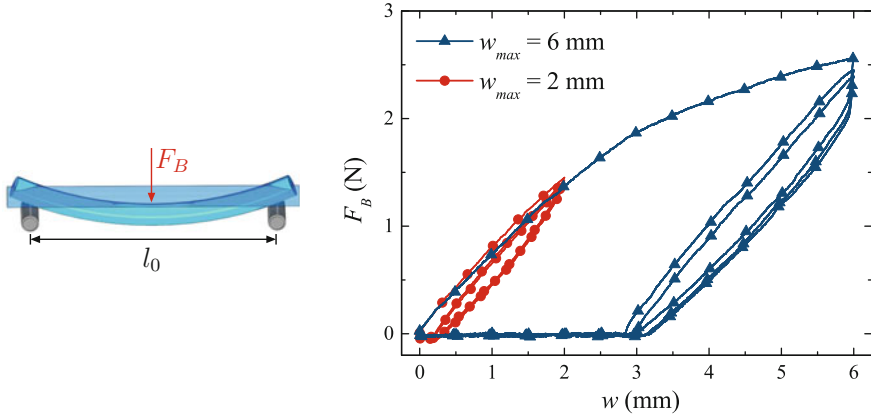


Fig. 3 Three point bending test: schematic drawing of the boundary conditions (**left**) and exemplary results of cyclic experiments on a cable showing elastic behavior for $w_{max} = 2$ mm and plastic behavior for $w_{max} = 6$ mm (**right**)

$$F_B(z = l_0/2) = 48 (EI)_B \frac{w(z = l_0/2)}{l_0^3}. \quad (3)$$

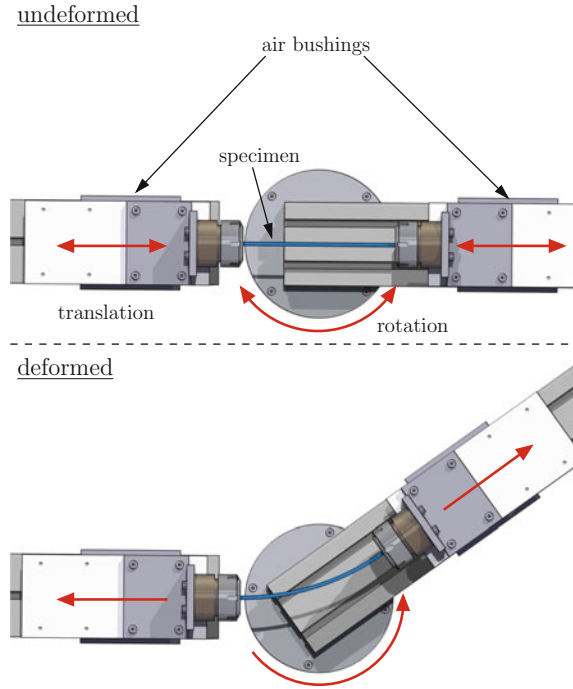
Figure 3 (right) shows an exemplary result of three point bending of a cable with a diameter of 2.8 mm and a free length between the supports of 56 mm. Again, results of different load ranges are displayed in order to illustrate the difference between cyclic loading in the elastic and inelastic range. Applying a deflection of 6 mm results in plastic hysteresis loops, where a bend in the first load curve implies the beginning of the plastic region. Furthermore, the specimen stays deflected during unloading so that the punch loses contact and force equals zero before the punch reaches the original position. Bending the specimen only up to a maximum deflection of 2 mm yields in contrast a smaller hysteresis, which lacks the plastic region. Additionally, no bend can be observed in the force-displacement diagram for small deflections.

Although this experiment is well-known and easily implemented, it has its limitations. First of all, it is only valid for small deflections and should therefore not be used for the investigation of large deformation effects like plasticity. Secondly, it provides only integrated information about the curvature and bending moment along the axis of the specimen, not their local values, which are the quantities that are relevant for the constitutive law for bending in this context, see Sect. 3.4. In order to get information about the local curvature, e.g. corresponding to the measured yield point, additional measurements such as optical deformation measurements are necessary.

Pure Bending Experiments

We designed a device which enables pure bending [2, 3] of a cable and therefore overcomes these limitations. The symmetrical experimental setup is shown in Fig. 4. In the undeformed state, the cable ends are clamped and mounted on slides. Air bushings ensure friction-free gliding of these slides along the axis of the specimen.

Fig. 4 Topview on the experimental setup for pure bending. The straight cable is clamped on slides which are mounted on friction-free air bushings. They allow for a translational motion of the specimen, while bending is realized by rotation of one cable end. Therefore, only a bending moment and no normal or shear forces act on the specimen



Thus, no normal forces act on the cable. Bending is realized by rotation of one of the cable ends. This setup guarantees that only a bending moment is applied on the specimen, i.e. no shear forces occur. The schematic boundary conditions are shown in Fig. 5 (left). These boundary conditions yield a configuration, where the bending moment M_B and the bending curvature K_B along the specimen are constant, i.e. the specimen's centerline is deformed to a circular arc. The specimen's bending curvature is then accessible as the inverse bending radius R of the specimen following basic geometry

$$K_B = \frac{1}{R}. \quad (4)$$

Calculating the stress distribution resulting from pure bending in the cross section of an Euler–Bernoulli beam under the assumptions of locally linear elastic material behavior, the bending moment can be derived as

$$M_B = (EI)_B K_B = \frac{EI}{R}. \quad (5)$$

Thus, the bending stiffness is in this experiment directly accessible as the slope of the elastic region of the bending moment over curvature diagram. An exemplary result of a cyclic pure bending experiment executed on a cable with a diameter of 2.8 mm and a

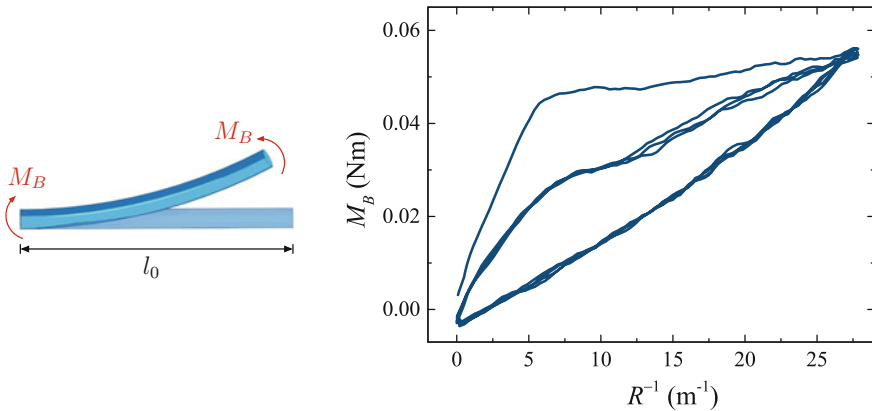


Fig. 5 Pure bending experiment: schematic drawing of the boundary conditions (**left**) and exemplary results of cyclic experiment on a cable showing plastic behavior for $\theta_{B,max} = 80^\circ$ (**right**)

free length of 50 mm is shown in Fig. 5 (right). Comparing it to Fig. 3 (right), the same elastoplastic characteristics are observable as in the three point bending experiment. The advantage of the pure bending experiment is the fact that the observed yield point is given as bending moment and corresponding bending curvature, which are directly the quantities that enter the constitutive law for bending, see Sect. 3.4.

Varieties in Constitutive Bending Behavior

Figures 6 and 7 show experimental results of both types of bending experiments on different beam-like specimens with circular cross sections in order to illustrate the varieties of constitutive bending behavior.

The diagrams shown in Fig. 6 result from cyclic three point and pure bending experiments on comparatively stiff, but elastic carbon fiber reinforced polymer (CFRP) rods of a diameter of 3 mm. The specimen used in the three point bending experiment had an initial free length of 170 mm and in the case of pure bending it had a free length of 410 mm. It is noticeable, that the loading paths are linear and coincide perfectly with the unloading paths in both bending experiments.

The results displayed in Fig. 7 show almost elastic, but nonlinear constitutive bending behavior. In contrast to elastoplastic behavior shown in Figs. 3 and 5, loading and unloading paths coincide – except for some viscous effects – and are parallel, but the slope of the curves changes during loading and unloading. These characteristics are called piecewise linear elastic bending behavior in this work. These diagrams result from bending experiments on Bowden cables with a special structural setup. They typically consist of an inner wire rope and a hollow housing of composite structure, which is incompressible in the longitudinal direction. The inner wire rope of the Bowden cables used in the experiments has a diameter of 2.1 mm and the housing has a diameter of 7.8 mm. In the three point bending experiment, an initial free length of 300 mm was used and in the pure bending experiment, the specimen

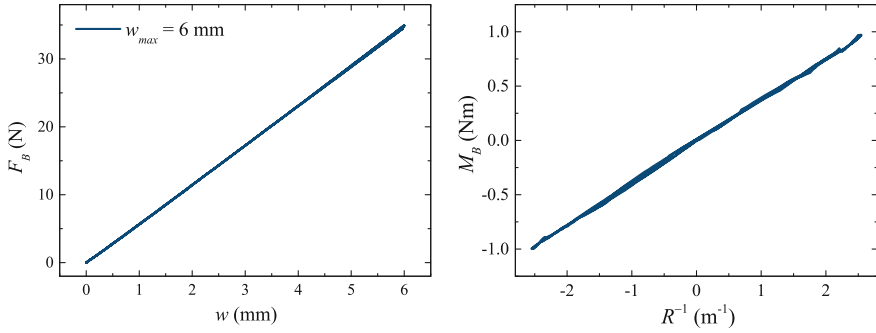


Fig. 6 Experimental results of cyclic bending experiments on elastic CFRP rods: three point bending with $w_{max} = 6$ mm (**left**) and pure bending with $\theta_{B,max} = \pm 60^\circ$ (**right**)

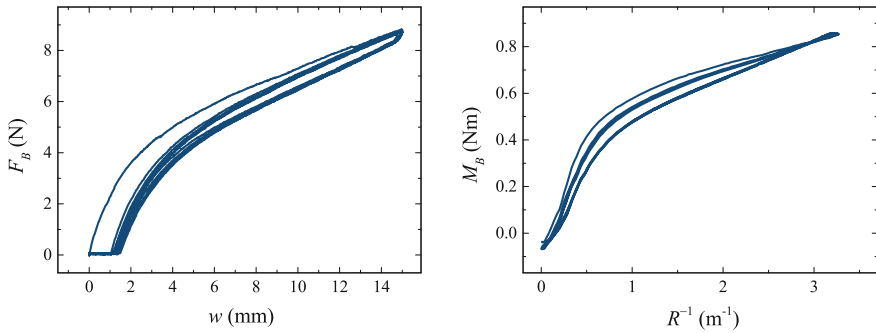


Fig. 7 Experimental results of cyclic bending experiments on Bowden cables showing nonlinear, approximately piecewise linear elastic behavior: three point bending with $w_{max} = 15$ mm (**left**) and pure bending with $\theta_{B,max} = 60^\circ$ (**right**)

had a free length of 320 mm. Bowden cables are commonly used, e.g. in bicycle brakes or motorcycle clutches, to transmit a tensile force.

It can be noticed, that the three point bending experiment as well as the pure bending experiment show the characteristics of the respective constitutive behavior, e.g. yield points, linear or nonlinear, elastic or inelastic behavior. The pure bending experiment, however, directly depicts the constitutive bending model as it shows the bending moment over bending curvature.

2.4 Discussion of Experiments

It was shown that the classical experiments for beam-like specimens can be used to characterize the rate independent behavior of elastoplastic cables under mechanical load.

Table 1 Elastic stiffnesses and Young's moduli calculated from the different classic experiments on a simple cable with a diameter of 2.8 mm

$(EA)_T$	$(E)_{Ten}$	$(GJ)_{Tor}$	$(E)_{Tor}$	$(EI)_B$	$(E)_B$
$7.96 \cdot 10^4 \text{ N}$	12900 MPa	$2.02 \cdot 10^{-3} \text{ Nm}^2$	1003.7 MPa	$1.37 \cdot 10^{-3} \text{ Nm}^2$	454.4 MPa

The elastic tensile, torsion and bending stiffnesses can be determined from linear fits to the elastic range of the corresponding experimental results. Table 1 shows the elastic stiffnesses that were determined from uniaxial tension, torsion and three point bending results given in the sections before. Under the assumptions of a circular, isotropic cross section and incompressible ($\nu = 0.5$) behavior, the Young's moduli were calculated from the respective stiffnesses by using

$$I = \frac{\pi}{4} R^4 = \frac{1}{2} J, \quad (6)$$

$$G = \frac{E}{2(1 + \nu)} = \frac{E}{3}. \quad (7)$$

They are also given in Table 1 in addition to the corresponding stiffness. The comparison of the Young's moduli that were determined from the three different types of experiments yields that the tensile stiffness is considerably higher than the torsional and bending stiffnesses. That means, the cable behaves much stiffer under tension than under torsion or bending due to the anisotropic inner structure of the cable. Consequently, it is not sufficient to determine the Young's modulus as the elastic material parameter for one cable, but one has to investigate the three different load cases separately and to determine the stiffnesses as a combination of material and structural parameters.

Different phenomena in the constitutive behavior are illustrated by the described experiments, especially when they are executed in consecutive cycles. The tensile, torsion and bending experiments on cables show the characteristics of elastoplastic behavior resulting from the multi-component structure. They appear due to inner friction or delamination of the constituents and the metal plasticity of the inner wires.

Furthermore, experimental results for different kinds of beam-like specimens illustrating the variety of constitutive bending behavior were shown. CFRP rods showing linear elastic behavior and Bowden cables showing piecewise linear elastic behavior were investigated in bending experiments exemplarily and will be discussed in Sect. 3.4 in more detail.

It has to be mentioned, that the described experiments only cover the three basic deformation modes for beam-like structures and are mostly uniaxial. In applications, however, mostly multiaxial deformations combining the basic deformations occur. First approaches in the experimental investigation of multiaxial deformations of cables are executed in [7], but are beyond the scope of this work.

3 Modeling of Flexible Beam-Like Structures for Virtual Product Development

The variety of experimental effects and different kinds of behavior shown in Sect. 2 can be modeled in the framework of continuum mechanics [9, 23]. It provides physically correct models to simulate the deformation of parts with a complex microstructure such as cables without having to take the microstructural properties explicitly into account. These properties certainly influence the deformation behavior of the cables strongly, but it is computationally and experimentally too expensive to include them into the model. We consequently aim for a model which is complex enough to cover the measured phenomena of cables under load and at the same time simple enough in the sense that its parameters are accessible in experiments.

The long and slender shape of the flexible parts provides the possibility to reduce the continuum model analytically to one dimension. These models are based on the Cosserat rod theory [20], which basically consists of three main parts: Geometrically exact kinematics that relate configuration variables with objective strain measures, balance equations that govern the equilibrium of the sectional forces and moments and constitutive laws giving the sectional quantities in terms of the deformation measures. The following subsections will describe them in detail.

3.1 Kinematics of Geometrically Exact Rods

The geometrically exact kinematics of a Cosserat rod are based on its configuration variables, see Fig. 8. The centerline curve is described by a space curve

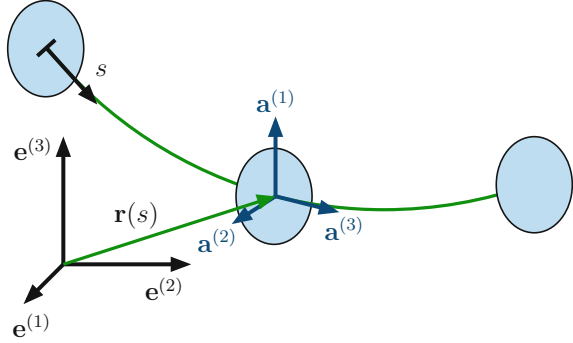
$$s \mapsto \mathbf{r}(s) \in \mathbb{R}^3, \quad (8)$$

and the orientation of the cross sections is given by a moving frame of orthonormal directors $\mathbf{a}^{(j)}(s)$

$$s \mapsto \mathbf{R}(s) = \mathbf{a}^{(j)}(s) \otimes \mathbf{e}_j \in SO(3), \quad (9)$$

both given as a function of the arc length parameter s [1]. The vectors $\mathbf{a}^{(1)}(s)$ and $\mathbf{a}^{(2)}(s)$ define the local cross section and $\mathbf{a}^{(3)} = \mathbf{a}^{(1)} \times \mathbf{a}^{(2)}$ is the cross section normal. The moving frame $\mathbf{R}(s)$ is called adapted to the curve if the tangent vector $\mathbf{t}(s) = \mathbf{r}'(s)$ equals $\mathbf{a}^{(3)}(s)$. This constraint is equivalent to the Euler–Bernoulli assumptions that cross sections remain orthogonal to the beam centerline and only a special case of the more general Cosserat curve which does not require this constraint.

Fig. 8 The kinematics of Cosserat rods



3.2 Deformation Measures

Based on the geometrically exact kinematics given in the section before, objective deformation measures can be defined. The rotational deformations \mathbf{K} and translational deformations $\mathbf{\Gamma}$ are given as vectors in the local coordinate system by

$$\begin{aligned} K^{(\alpha)} &:= \langle \mathbf{a}^{(\alpha)}, \mathbf{a}^{(3)} \times \partial_s \mathbf{a}^{(3)} \rangle; & \Gamma^{(\alpha)} &:= \langle \mathbf{a}^{(\alpha)}, \partial_s \mathbf{r} \rangle; & \alpha &= 1, 2 \\ K^{(3)} &:= \langle \mathbf{a}^{(2)}, \partial_s \mathbf{a}^{(1)} \rangle; & \Gamma^{(3)} &:= \langle \mathbf{a}^{(3)}, \partial_s \mathbf{r} \rangle - 1, \end{aligned} \quad (10)$$

where $\langle \bullet, \bullet \rangle$ is the scalar product. The components $K^{(\alpha)}$ give the curvatures for bending about the axes defined by $\mathbf{a}^{(\alpha)}$ and $K^{(3)}$ measures the torsional twist. The bending curvatures can be combined in the vector $\mathbf{K}_B = (K^{(1)}, K^{(2)})^T$ and its length

$$K_B = \|\mathbf{K}_B\| = \sqrt{(K^{(1)})^2 + (K^{(2)})^2} \quad (11)$$

is the absolute value of the bending curvature. The entries $\Gamma^{(\alpha)}$ measure the transverse shear strains and the longitudinal strain, relevant for uniaxial tension, is denoted by $\Gamma^{(3)}$.

3.3 Static Equilibrium Equations

In analogy to the deformation measures, the sectional quantities can be divided in translational sectional quantities, the sectional forces \mathbf{F} , and rotational sectional quantities, the sectional moments \mathbf{M} . The components $F^{(1,2)}$ of the sectional forces are in accordance with the translational deformation measures the transverse shear forces and $F^{(3)}$ is the longitudinal force which is equivalent to the force measured in the uniaxial tensile test. The moments resulting from bending about the bending axes are consequently $M^{(1,2)}$ and the torsional moment is given by $M^{(3)}$. Equivalently to the bending curvature given in (11), the bending moments can be summarized in the

vector $\mathbf{M}_B = (M^{(1)}, M^{(2)})^T$ and the absolute value of the bending moment is given by the vector's length

$$M_B = \|\mathbf{M}_B\| = \sqrt{(M^{(1)})^2 + (M^{(2)})^2}. \quad (12)$$

Vectors denoted with a capital letter are material quantities, i.e. defined in the local coordinate system of the beam. The static equilibrium equations, however, can be formulated more neatly in the spatial sectional quantities, defined in the global coordinate system. They can be calculated from the material sectional quantities by using the moving frame according to

$$\mathbf{f} = \mathbf{R}(s) \cdot \mathbf{F}; \quad \mathbf{m} = \mathbf{R}(s) \cdot \mathbf{M}. \quad (13)$$

The system of static equilibrium equations for Cosserat rods is then given as

$$\begin{aligned} \partial_s \mathbf{f} + \mathbf{f}_{ext} &= \mathbf{0}, \\ \partial_s \mathbf{m} + \partial_s \mathbf{r} \times \mathbf{f} + \mathbf{m}_{ext} &= \mathbf{0}. \end{aligned} \quad (14)$$

The vectors \mathbf{f}_{ext} and \mathbf{m}_{ext} denote external forces and moments acting on the axis of the Cosserat rod.

3.4 Constitutive Laws

The continuum mechanical framework for the simulation of flexible, slender parts like cables is given in the previous sections, except for the constitutive equations. We will focus on these now since they provide the possibility to model different kinds of deformation behavior [14]. In contrast to a general three-dimensional formulation in tensor quantities, constitutive laws for Cosserat rods can be formulated in the vectors of the sectional quantities due to their slender geometry [10, 15, 17]. This is especially of advantage in regard of experiments. The sectional quantities are in most cases the measured quantities in the classical experiments for beams, which enables the investigation of the constitutive behavior directly in the experiments without the necessity for reverse engineering. In the following, the modeling of three types of rate independent constitutive behavior is described in more detail: linear elasticity, piecewise linear elasticity and elastoplasticity.

Linear Elasticity for Cosserat Rods

In the simplest case of linear elasticity the stress tensor σ is related linearly to the strain tensor \mathbf{E} via the elastic stiffness tensor \mathbb{C} in three dimensions

$$\sigma = \mathbb{C} : \mathbf{E}, \quad (15)$$

which is known as Hooke's law. It can be formulated equivalently for the material sectional quantities of the Cosserat rod as

$$\mathbf{F} = \mathbb{C}_F \cdot \mathbf{F}_{el}; \quad \mathbf{M} = \mathbb{C}_M \cdot \mathbf{K}_{el}, \quad (16)$$

where the effective elastic stiffness matrices are given by

$$\mathbb{C}_F = \begin{bmatrix} (GA)_1 & 0 & 0 \\ 0 & (GA)_2 & 0 \\ 0 & 0 & (EA)_T \end{bmatrix}; \quad \mathbb{C}_M = \begin{bmatrix} (EI)_1 & 0 & 0 \\ 0 & (EI)_2 & 0 \\ 0 & 0 & (GJ)_T \end{bmatrix}. \quad (17)$$

In case of isotropic circular cross sections, the bending stiffnesses are equal and denoted as $(EI)_1 = (EI)_2 = (EI)_B$. The same applies to the transverse shear stiffnesses, i.e. $(GA)_1 = (GA)_2 = (GA)_S$, which cannot be easily determined in experiments. It is, however, valid to calculate them from the other experimentally determined stiffnesses as the transverse shear is small in parts with a high aspect ratio.

An experimental result for linear elastic bending behavior is displayed in Fig. 6. The diagram resulting from pure bending on the right hand side directly illustrates the linear elastic constitutive law for bending of a specimen with a circular isotropic cross section in the plane,

$$M_B = (EI)_B K_B. \quad (18)$$

It is visible, that loading and unloading paths coincide, which means no energy is lost in this process and it is reversible. Only few beam-like specimens, such as the CFRP rods, behave linearly elastic at finite deformations. In most cases, linear elasticity is only observed at small deformations. Material nonlinearities, in contrast to the already introduced geometrical nonlinearities covered by the geometrically exact kinematics, have to be considered then.

Piecewise Linear Elasticity for Bending of Cosserat Rods

A different kind of reversible, rate independent, behavior is shown in Fig. 7: Piecewise linear elasticity in bending. This type of constitutive behavior has only been observed in bending experiments on Bowden cables, so far. It is still interesting to investigate in pure bending, since the constitutive behavior can be depicted directly in this experiment.

The characteristics of piecewise linear elastic bending behavior are portrayed schematically in Fig. 9 (left). The diagram of bending moment over bending curvature shows linear elastic bending with a bending stiffness $(EI)_{B,1}$ up to a certain threshold curvature $K_{B,t}$. At this point, the slope of the graph, i.e. the bending stiffness, changes to $(EI)_{B,2}$. The unloading path follows the same behavior and coincides with the loading path, no hysteresis occurs. The real results obtained in a pure bending experiment corresponding to this ideal behavior are shown in Fig. 7 (right). Obviously, the threshold curvature is not as clearly detectable as in theory and a small hysteresis, probably due to viscous material behavior or plastic structural

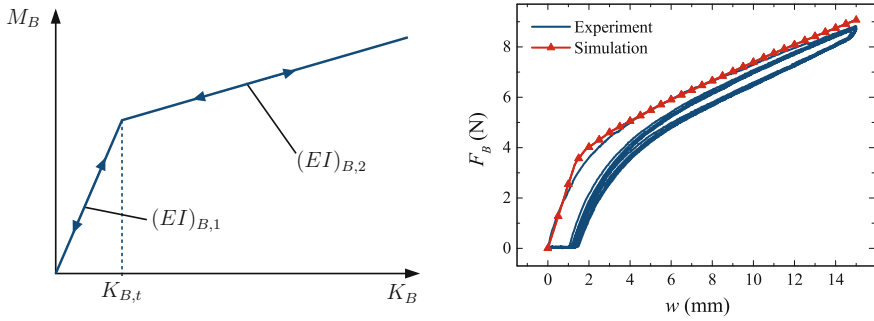


Fig. 9 Schematic drawing of piecewise linear elastic bending constitutive law (**left**) and comparison of experimental results of three point bending on a Bowden cable with simulation results using piecewise linear elastic bending (**right**)

Table 2 Experimentally determined model parameters for piecewise linear elastic bending model

Bending stiffness $(EI)_{B,1}$	Bending stiffness $(EI)_{B,2}$	Threshold curvature $K_{B,t}$
1.40 Nm^2	0.19 Nm^2	0.18 m^{-1}

effects, occurs. However, it is evident that the bending stiffness is higher at smaller curvatures and that the behavior is reversible.

This piecewise linear elasticity can simply be modeled by distinction of the cases

$$M_B = \begin{cases} (EI)_{B,1} K_B & \text{for } |K_B| < K_{B,t} \\ M_{B,t} + (EI)_{B,2} (K_B - K_{B,t}) & \text{for } |K_B| \geq K_{B,t}, \end{cases} \quad (19)$$

with the threshold bending moment $M_{B,t} = (EI)_{B,1} K_{B,t}$. The results of the simulation of a three point bending experiment with this kind of model are shown in Fig. 9 (right) in comparison with the experimental results of three point bending. The experimentally determined model parameters are given in Table 2. It has to be mentioned, that the curve resulting from simulation shows one complete cycle, i.e. loading and unloading. This is not visible, because the loading and unloading paths coincide. The experimental and simulated results show good agreement, except for a small hysteresis in the experiment which is probably caused by viscous or damage effects that are not covered in the model. The simple formulation of piecewise defined elastic bending stiffnesses at least models the loading behavior of Bowden cables in three point bending very well.

Elastoplasticity for Cosserat Rods

The results from cyclic experiments on simple cables given in Sects. 2.1, 2.2 and 2.3 illustrated strongly nonlinear and inelastic behavior under the three basic deformations. A rate independent elastoplastic constitutive law allows for the integration of the various underlying material and structural effects, such as metal plasticity,

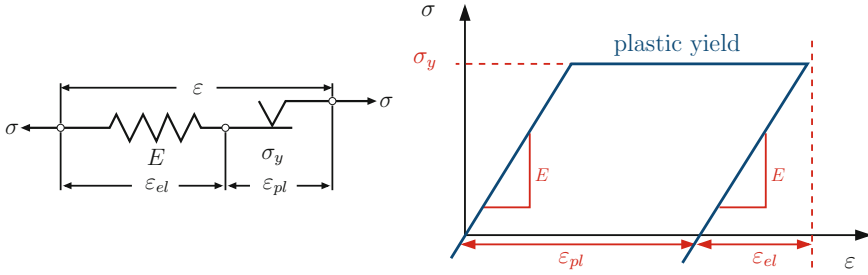


Fig. 10 Illustration of a one-dimensional rate independent elastoplastic rheological model, according to [21] (left) and a schematic stress-strain-diagram for one-dimensional perfect elastoplasticity (right)

friction between the constituents, delamination and damage without the necessity of investigating them on the microstructural level.

The rheological model shown in Fig. 10 illustrates the simplest case of one-dimensional elastoplasticity [21]. It consists of a linear elastic spring with Young's modulus E which is serially connected to a Coulomb friction element with yield point σ_y . The total strain ε can be split additively into an elastic part ε_{el} and a plastic part ε_{pl} , when the whole device is loaded with the stress σ . Starting at the linear elastic constitutive law,

$$\sigma = E \varepsilon_{el}, \quad (20)$$

and using the additive split of the total strain,

$$\varepsilon = \varepsilon_{el} + \varepsilon_{pl}, \quad (21)$$

the elastoplastic constitutive law can be formulated as

$$\sigma = E (\varepsilon - \varepsilon_{pl}). \quad (22)$$

The resulting stress-strain-curve is given schematically in Fig. 10 (right).

In our case of very slender objects, it is valid to transfer this simple concept to the deformation measures of the Cosserat rod, since the local deformations remain small, even if the global displacements and rotations are large. Otherwise, an additive split of the deformation measures would not suffice and a multiplicative split should be used. In analogy to (20), (21), (22), the deformation measures of the Cosserat rod are split into an elastic and a plastic part,

$$\mathbf{\Gamma} = \mathbf{\Gamma}_{el} + \mathbf{\Gamma}_{pl}; \quad \mathbf{K} = \mathbf{K}_{el} + \mathbf{K}_{pl}, \quad (23)$$

and the elastoplastic constitutive laws for the sectional forces and moments are

$$\begin{aligned} \mathbf{F} &= \mathbb{C}_{\mathbf{F}} \cdot \boldsymbol{\Gamma}_{el}; & \mathbf{M} &= \mathbb{C}_{\mathbf{M}} \cdot \mathbf{K}_{el}, \\ \mathbf{F} &= \mathbb{C}_{\mathbf{F}} \cdot (\boldsymbol{\Gamma} - \boldsymbol{\Gamma}_{pl}); & \mathbf{M} &= \mathbb{C}_{\mathbf{M}} \cdot (\mathbf{K} - \mathbf{K}_{pl}). \end{aligned} \quad (24)$$

In order to describe the onset of plastic yield, i.e. the limits of the elastic region, a yield criterion has to be defined. At first, we consider the case of perfect plasticity, where no hardening occurs. It is assumed, that the stress in the elastoplastic device cannot exceed the yield point σ_y and consequently, all admissible stress states have to be smaller than or equal to σ_y . In the most general case, the yield condition is then formulated as

$$f(\sigma) := |\sigma| - \sigma_y \leq 0. \quad (25)$$

We can distinguish two cases in (25). As long as $f(\sigma) < 0$ is satisfied, the response of the device is instantaneous and elastic. The plastic strain does not change in this case, i.e. $\dot{\varepsilon}_{pl} = \partial \varepsilon_{pl} / \partial t = 0$. When $f(\sigma) = 0$ and a loading condition is fulfilled, the Coulomb friction element is active and plastic yield occurs. Consequently, the plastic strain changes and $\dot{\varepsilon}_{pl} \neq 0$. The change of the plastic strain is then described by an evolution equation called flow rule. If the flow rule is connected to the yield condition by

$$\dot{\varepsilon}_{pl} = \gamma \frac{\partial f}{\partial \sigma}, \quad (26)$$

i.e. the flow potential is equal to the yield condition, the flow rule is called associative. While the derivative $\partial f / \partial \sigma$ determines the direction of plastic flow, the proportionality factor γ gives the absolute value of the plastic strain rate. It can be calculated from the consistency condition

$$\gamma \dot{f}(\sigma) = 0, \text{ if } f(\sigma) = 0, \quad (27)$$

which states that if plastic flow occurs, the stress state has to remain on the yield surface, i.e. the value $f = 0$ does not change during yield. The necessary requirements for yielding can be summarized in the Kuhn–Tucker complementarity conditions, see e.g. [16],

$$\gamma \geq 0; \quad f(\sigma) \leq 0; \quad \gamma f(\sigma) = 0. \quad (28)$$

In the following, we will focus on elastoplastic bending behavior, since this is the deformation mode most common regarding plasticity in applications of cables. The elastoplastic constitutive law for bending is formulated in analogy to (24), using the vectorial bending curvature and moment as

$$\mathbf{M}_B = (EI)_B (\mathbf{K}_B - \mathbf{K}_{B,pl}). \quad (29)$$

The experimental results in Sect. 2.3 showed elastoplastic behavior in three point bending, as well as in pure bending experiments on cables. If one compares the first load cycles in Figs. 3 and 5 to the illustration of perfect elastoplasticity in Fig. 10, it is evident, that perfect plasticity will not enable the modeling of the observed behavior.

During yield in the first load cycle, (strain) hardening occurs in the experiments, i.e. the bending moment increases after the yield point is reached.

In order to include hardening in the plasticity formulation, further internal variables in addition to the plastic strain have to be introduced. We will describe the simple case of linear isotropic strain hardening, since it seems to be sufficient to describe the first loading of the pure bending experiment shown in Fig. 5. The yield condition in one dimension is then given by

$$f(\sigma, \mathbf{q}) := |\sigma| - [\sigma_y + H\alpha] \leq 0, \quad \alpha \geq 0, \quad (30)$$

with the internal hardening variable α , the hardening modulus H and the vector of internal variables \mathbf{q} . This yield condition describes isotropic hardening behavior, because the center of the elastic region does not change its position, but it expands isotropically. The evolution of α is given by the hardening law, which can be formulated as an associative evolution equation, as well,

$$\dot{\alpha} = \gamma \frac{\partial f(\sigma, \mathbf{q})}{\partial \mathbf{q}}. \quad (31)$$

The equivalent yield function for linear isotropic hardening for bending of a Cosserat rod can be formulated as

$$f(M_B, \mathbf{q}) := M_B - [M_{B,y} + (HI)_B \alpha] \leq 0, \quad \alpha \geq 0, \quad (32)$$

using the effective bending moment given in (12). The yield point in bending is called $M_{B,y}$ and $(HI)_B$ is the hardening modulus for bending. In analogy to the bending stiffness $(EI)_B$, the area moment of inertia I is included into the definition of the hardening modulus. This yield function can be interpreted as a circle in the bending moment plane with a radius of $M_{B,y}$, which is suitable for homogeneous, isotropic and circular cable cross sections. It is shown in Fig. 11 (right). The resulting moment-curvature-diagram for pure bending is depicted in Fig. 11 (left). Comparing this theoretical diagram to the real experimental results of pure bending given in Fig. 5, it is evident that this formulation will enable the description of the first load path. The unloading in the experiment, however, deviates from the theoretical diagram, since it is not parallel to the elastic loading path. This indicates, that the inelastic effects in the experiment cannot be covered completely by an elastoplastic formulation. In [8], numerical experiments using the elastoplastic formulation with isotropic hardening given by (27)–(29), (31) and (32) are executed. For this purpose, a finite beam element based on Cosserat rod theory is derived and used for the simulation of three point bending and pure bending experiments of a cable. The comparison of the simulation results to the experimental results confirms the presumption that the elastoplastic formulation is not sufficient to model the unloading path in pure bending experiments. However, the change in stiffness during unloading can be modeled using an additional pseudo-damage formulation based on the sectional quantities of the Cosserat rod. This extension exceeds the scope of this work, but it is treated in detail in [8].

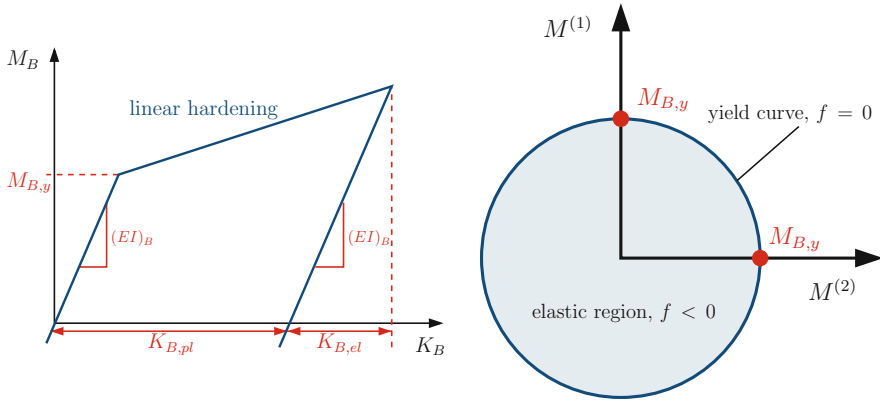


Fig. 11 Schematic illustration of elastoplastic bending behavior with linear hardening (**left**) and schematic drawing of a yield function in the bending moment plane (**right**)

It has to be noted that this formulation for elastoplastic bending does not account for coupling of the bending moment with the remaining sectional quantities of the Cosserat rod, i.e. tension and torsion. We assume that they stay in the elastic region and do not influence the bending plasticity, which is valid for the considered planar pure bending experiment. It is, however, only the first step towards describing the three-dimensional deformation behavior of cables showing inelastic behavior.

4 Conclusions

This chapter combines experimental work and theoretical considerations regarding the constitutive modeling of the deformation behavior of cables.

Since cables are slender and flexible, they can be characterized by means of classical experiments for beam-like structures. Section 2 treated experiments covering the three basic deformation modes of beams: tension, torsion and bending. In addition to the well-known uniaxial tension test, torsions test and three point bending experiment, a new device which enables the pure bending of cables, was introduced. It was shown, that the anisotropic and inhomogeneous structure of the cable demands for the use of stiffness parameters for the respective load cases in order to completely describe the elastic deformation behavior of the cable. It is not sufficient to determine only a material property, such as the Young's modulus E , to cover the behavior of a cable under load. Moreover, it was shown that the constitutive behavior, even of simple cables, exceeds linear elasticity. The multi-component structure of the cable causes inelastic effects, e.g. friction, damage or delamination, which is superposed by inelastic material effects such as metal plasticity of the conducting wires. Results of experiments executed on different kinds of beam-like specimens – CFRP rods and Bowden cables – illustrated the varieties in constitutive behavior with a focus on bending. The

differences between linear elastic, piecewise linear elastic and elastoplastic bending behavior were depicted.

The slender geometry of cables allows for the reduction of the three-dimensional framework of continuum mechanics to one dimension. In Sect. 3, a brief summary of the Cosserat rod theory, which enables the constitutive modeling in terms of the sectional forces and moments of the beam, was given. This reduction not only simplifies the complexity of the model and therefore reduces the numerical effort, but it also corresponds very well to the experiments for beam-like structures. The sectional quantities of the Cosserat rod model correspond (most often) to the quantities measured in the experiments. Therefore, one may directly utilize experimental results as those given in Sect. 2 to deduce suitable constitutive models for Cosserat rods, as demonstrated in the particular examples describing linear elastic, piecewise linear elastic and elastoplastic bending behavior.

References

1. Antman, S.S.: *Nonlinear Problems of Elasticity*. Springer, Berlin (2005)
2. Balke, H.: *Einführung in die Technische Mechanik*. Springer, Berlin (2008)
3. Beer, F.P., Johnston, E.R.: *Mechanics of Materials*. McGraw-Hill, London (1992)
4. Costello, G.A., Phillips, J.W.: Effective modulus of twisted wire cables. *J. Eng. Mech. Div.* **102**(1), 171–181 (1976)
5. Costello, G.A., Sinha, S.K.: Torsional stiffness of twisted wire cables. *J. Eng. Mech. Div.* **103**(4), 766–770 (1977)
6. Dörlich, V., Diebels, S., Linn, J.: Investigation of elastoplastic effects of cables under large spatial deformation. *Proc. Appl. Math. Mech.* **15**, 185–186 (2015)
7. Dörlich, V., Linn, J., Scheffer, T., Diebels, S.: Towards viscoplastic constitutive models for cosserat rods. *Arch. Mech. Eng.* **63**, 215–230 (2016)
8. Dörlich, V., Češarek, P., Linn, J., Diebels, S.: Experimental investigation and numerical modeling of resultant-based bending plasticity in cables. In: *Proceedings of 8th ECCOMAS Thematic Conference on Multibody Dynamics*, Prague (2017)
9. Gurtin, M.E.: *An Introduction to Continuum Mechanics*. Academic Press, New York (1981)
10. Han, S., Bauchau, O.A.: Nonlinear, three-dimensional beam theory for dynamic analysis. In: *Multibody System Dynamics*, pp. 1–28 (2016)
11. Haupt, P.: *Continuum Mechanics and Theory of Materials*. Springer Science & Business Media (2013)
12. Hoeft, F., Stephan, T., Hermanns, O.: Eine neue Methode zur vergleichenden örtlichen Beanspruchungsanalyse für Kabel und Schläuche. *SIMVEC Berechnung und Simulation im Fahrzeugbau, VDI Berichte* **2107**, 297–309 (2010)
13. Knapp, R.H.: Derivation of a new stiffness matrix for helically armoured cables considering tension and torsion. *Int. J. Numer. Meth. Eng.* **14**(4), 515–529 (1979)
14. Lemaitre, J., Chaboche, J.L.: *Mechanics of Solid Materials*. Cambridge university press, Cambridge (1994)
15. Linn, J., Lang, H., Tuganov, A.: Geometrically exact Cosserat rods with Kelvin–Voigt type viscous damping. *Mech. Sci.* **4**(1), 79–96 (2013)
16. Luenberger, D.C.: *Linear and Nonlinear Programming*. Addison-Wesley Publishing Company, Reading (1984)
17. Mata, P., Oller, S., Barbat, A.H.: Static analysis of beam structures under nonlinear geometric and constitutive behavior. *Comput. Methods Appl. Mech. Eng.* **196**(45), 4458–4478 (2007)

18. Reissner, E.: On one-dimensional large-displacement finite-strain beam theory. *Stud. Appl. Math.* **52**, 87–95 (1973)
19. Schneider, F., Linn, J., Hermansson, T., Andersson, F.: Cable dynamics and fatigue analysis for digital mock-up in vehicle industry. In: *Proceedings of 8th ECCOMAS Thematic Conference on Multibody Dynamics*, Prague (2017)
20. Simo, J.C.: A finite strain beam formulation: the three dimensional dynamic problem - Part I. *Comput. Meth. Appl. Mech. Eng.* **49**(1), 55–70 (1985)
21. Simo, J.C., Hughes, T.J.R.: *Computational Inelasticity*. Springer, New York (1998)
22. Timoshenko, S.P., Gere, J.M.: *Mechanics of Materials*. Van Nostrand Reinhold Company, New York (1972)
23. Truesdell, C., Noll, W.: In: Antman, S.S. (ed.) *The Non-linear Field Theories of Mechanics*, 3rd edn. Springer, Berlin (2004)
24. Vaz, M.A., Aguiar, L.A.D., Estefen, S.F., Brack, M.: Experimental determination of axial, torsional and bending stiffness of umbilical cables. In: *Proceedings of 17th International Conference on Offshore Mechanics and Arctic Engineering* (1998)
25. Witz, J.A., Tan, Z.: Rotary bending of marine cables and umbilicals. *Eng. Struct.* **17**(4), 267–275 (1995)

Advances in Mechanics of Materials and Structural
Analysis

In Honor of Reinhold Kienzler

Altenbach, H.; Jablonski, F.; Müller, W.H.; Naumenko, K.;
Schneider, P. (Eds.)

2018, X, 461 p. 226 illus., 160 illus. in color., Hardcover
ISBN: 978-3-319-70562-0